Calcified plaque modification alters local drug delivery in the treatment of peripheral atherosclerosis

Abraham R. Tzafriri, PhD[1,2], **Fernando Garcia-Polite, PhD**[1,2], **Brett Zani, PhD**[1], **James Stanley, DVM, MS, PhD**[1], **Benny Muraj, MV**[1], **Jennifer Knutson, BS**[1,3], **Robert Kohler, MS**[3], **Peter Markham, MS**[1], **Alexander Nikanorov, MD, PhD**[3], and **Elazer R. Edelman, MD, PhD**[2,4]

[1]CBSET Inc, 500 Shire Way, Lexington MA, USA

[2]IMES, MIT, 77 Massachusetts Avenue Cambridge, MA, USA

[3]Cardiovascular Systems, Inc, 1225 Old Hwy 8NW, Saint Paul, MN, USA

[4]Cardiovascular Division, Brigham and Women's Hospital, Harvard Medical School, Boston, MA, USA

Abstract

Background—Calcific atherosclerosis is a major challenge to intraluminal drug delivery in peripheral artery disease (PAD).

Objectives—We evaluated the effects of orbital atherectomy on intraluminal paclitaxel delivery to human peripheral arteries with substantial calcified plaque.

Methods—Diagnostic angiography and 3-D rotational imaging of five fresh human lower limbs revealed calcification in all main arteries. The proximal or distal segment of each artery was treated using an orbital atherectomy system (OAS) under simulated blood flow and fluoroscopy. Explanted arterial segments underwent either histomorphometric assessment of effect or tracking of ^{14}C-labeled or fluorescent–labeled paclitaxel. Radiolabeled drug quantified bulk delivery and fluorescent label established penetration of drug over finer spatial domain in serial microscopic sections. Results were interpreted using a mathematical model of binding-diffusion mediated arterial drug distribution.

Results—Lesion composition affected paclitaxel absorption and distribution in cadaveric human peripheral arteries. Pretreatment imaging calcium scores in control femoropopliteal arterial segments correlated with a log-linear decline in the bulk absorption rate-constant of ^{14}C-labeled, declining 5.5-fold per calcified quadrant (p=0.05, n=7). Compared to controls, OAS-treated femoropopliteal segments exhibited 180μm thinner intima (p<0.001), 45% less plaque calcification, and 2 log orders higher paclitaxel bulk absorption rate-constants. Correspondingly, fluorescent paclitaxel penetrated deeper in OAS-treated femoropopliteal segments compared to controls, due to a 70% increase in diffusivity (p<0.001).

Corresponding author: Rami Tzafriri, PhD, CBSET Inc., 500 Shire Way, Lexington, MA, 02421, Phone: 781-541-5589, Fax: 781-541-5656.

Conclusions—These data illustrate that calcified plaque limited intravascular drug delivery, and controlled OAS treatment of calcific plaques resulted in greater drug permeability and improved adjunct drug delivery to diseased arteries.

Keywords

Introduction

Considerable progress has been made in interventional treatments of peripheral artery disease (PAD), yet key challenges remain that are largely attributed to lesion morphology and calcific burden[1]. While percutaneous transluminal angioplasty relies on plaque fracture and vessel wall stretching[2], calcium alters morphology and compliance of the arterial wall reducing the effect of both angioplasty and stent deployment. Moreover, calcification increases the occurrence of flow limiting dissections and acute vessel recoil[3], and limits stent efficacy by increasing the risk of incomplete stent expansion, malapposition, and fractures[4]. Paclitaxel coated balloons (PCB) reduce restenosis in the superficial femoral and popliteal arteries but have not been proved to be effective in below-the-knee arteries[5, 6]. Fanelli et al.[7] observed that late lumen loss and primary patency 12 months following PCB treatment correlated negatively with the degree of circumferential calcification as assessed by computerized tomographic angiography, and hypothesized that vessel wall calcification impedes paclitaxel absorption. These and other investigators have suggested that vessel preparation by atherectomy might remove barriers to intravascular drug absorption and distribution in the artery wall[8]. Arterial plaque can be removed by a range of intravascular atherectomy devices[9] that excise it using cutting blades (directional atherectomy) or sand it down via high speed concentric rotation of a diamond-encrusted elliptical burr (rotational atherectomy) or an eccentric crown that orbits along a spiral path and frictionally pulverizes hard surfaces into harmless microparticles (orbital atherectomy).

Data on adjunctive directional atherectomy and PCB from a single-center non-randomized study[10] looked promising, and additional studies are underway. However, clinical experience with adjunctive rotational atherectomy and coronary drug eluting stents has been mixed[11–14] and it remains unclear whether atherectomy did not enhance drug delivery or whether such benefits existed but were counterbalanced by restenotic response to the atherectomy related injuries[12]. Preclinical experiments are better suited for examining the barrier effect of plaque on drug absorption and distribution with or without atherectomy. Unfortunately, induction of mineralization in animal models has proven difficult and a recent study in atheromatous arteries in the pig model exhibited comparable paclitaxel deposition 30 days post PCB treatment in OAS-pretreated vs native femoral arteries[15].

The current study was designed to directly quantify the intravascular absorption and distribution of paclitaxel in calcific human peripheral arteries at baseline and after OAS treatment. This design allowed the quantification of the barrier properties of calcific intimal plaque on paclitaxel absorption and its modulation by arterial plaque modification in

femoropoliteal arteries. The study was not designed to address the impact of medial calcification on drug absorption. Limited observations on drug delivery in calcified tibial arteries are reported to help with future study designs.

Methods

Experimental overview

Five fresh human lower limbs were obtained from a certified research institution and maintained on ice for further evaluation. 3-D rotational imaging (GE Healthcare Innova® 2100 Cath Lab, Milwaukee, Wisconsin, USA) was performed on all limbs to identify the distribution and severity of calcification in the lower extremity arteries. Intra-arterial sheaths were inserted proximally and distally to simulate human arterial blood flow with saline perfusion. Under fluoroscopic guidance, a guiding catheter was advanced through the sheath into designated peripheral arteries and angiographic images were obtained to identify lesion location for OA. The superficial femoral arteries (SFA), popliteal and tibial arteries were divided through angiographic measurements into approximately equal segment lengths, and the proximal or distal segment of each artery was treated using the DIAMONDBACK 360® OAS (Cardiovascular Systems, Inc., Saint Paul, MN) with Solid Crowns (1.25 - 2.0 mm), delivered as 3 consecutive OAS runs, at 60,000 rpm, 90,000 rpm and 120,000 rpm in 60-140 mm long lesions (91.7±6.7 mm).

After OAS treatment, arteries were harvested and divided into 2-8 cm long tubular segments. Each segment was annotated relative to the location of the OAS treatment site, and assigned for histology, scanning electron microscopy (SEM), or drug incubation with ^{14}C-labeled paclitaxel for drug uptake analysis or fluorescent labeled paclitaxel for drug distribution analysis as described below (Fig 1). Segments assigned for drug incubation were retrospectively scored for circumferential calcium burden based on 3-D images or angiography. Following Fanelli et al.[7], a score of 1-4 was assigned based on the number of quadrants exhibiting substantial calcification.

Drug incubation

Freshly excised arterial segments (3-8 cm long) originating from OAS-treated or untreated sites were trimmed to reduce edge effects, ligated with suture at one end (as were any side branches) and lumenally infused with a buffered solution (PBS/4% BSA) of radiolabeled (^{14}C, 10 μM) or fluorescent (Oregon Green 488, 10 μM) paclitaxel. Fully infused arterial segments were ligated in the open end and incubated in 50 mL PBS/4% BSA (37^{0}C) in a shaking water bath. After 1h, incubated segments were rinsed with PBS to remove residual unbound drug, and processed for scintillation counting or fluorescent microscopy.

Analysis of radiolabeled drug uptake

After drug infusion, the sutured ends of each vessel were cut away, and the artery flushed with PBS to remove residual, unbound ^{14}C paclitaxel (Fig 2A). Wash and incubation solution volumes were recorded for each artery and analyzed for isotope activity. The sutured ends and remaining segment (~1.5-2.5 cm) of each artery were weighed and incubated in excess Solvable® (Perkin Elmer) at 37°C in a shaking water bath. Digested

samples were analyzed for 1-2 minutes for isotope activity in a liquid scintillation counter. Scintillation counts were converted to drug weight and divided by tissue weight to obtain the bulk tissue content for each artery. Drug tissue content (M_{tissue}) was normalized to the (leakage corrected) infused drug dose (M_{dose}), and contrasted with the diffusion-binding model predicted uptake kinetics from a finite volume (Fig 2B):

$$M_{tissue}(t)/M_{dose} = 1 - e^{k_{uabsorb}t}\operatorname{erfc}\left(\sqrt{k_{absorb}t}\right), \quad k_{absorb}t < 1 \quad (1)$$

where

$$k_{absorb} \equiv \frac{D_{eff}(k_p f_u)^2}{(V_{lumen}/A_{mural})^2} \quad (2)$$

is a bulk absorption rate-constant, D_{eff} is the effective diffusion coefficient of drug in the penetrated tissue layer, k_p is the equilibrium partition coefficient of the drug in the tissue, f_u is the fraction of free drug in the infusate, V_{lumen} is the volume of infusate and A_{mural} is the mural surface area of the tissue, estimated by assuming a cylindrical lumen. The derivation and numerical validation of Eqs. 1–2 is detailed in the Supplemental methods (Figs S1-S4). Evaluation of the right hand side of Eq. 1 at t=1hr provided an estimate of the bulk absorption rate-constant k_{absorb}. For an inhomogeneous tissue, supplemental numerical simulations illustrate that the estimated k_{absorb} is representative of the spatially averaged effective diffusion coefficient (Fig S4C, Supplemental methods).

Analysis of Fluorescent drug distribution

After drug infusion, the sutured ends of each vessel were excised and discarded. The remaining artery segments were flushed with PBS and embedded in OCT tissue freeze medium and snap frozen. Embedded arterial segments were cryosectioned to yield 0.010 mm thick parallel cross-sections with a cryostat (Thermo Electron Cryotome SME, Waltham, Massachusetts, USA), stored at −20°C, and subsequently imaged on an OLYMPUS BX60 epifluorescence microscope running cellSens 1.4 (Olympus Optical Corporation, Ltd., Tokyo, Japan).

Using ImageJ (NIH, Bethesda, Maryland, USA) the lumen of images of fluorescent arterial sections was extracted, a luminal centroid estimated, and a zero intensity baseline established to account for autofluorescence. Fluorescent drug intensity profiles were assessed in 10° increments circumferentially. The penetration depth at each angle was defined as the distance from the lumen at which intensity declined to 10% of peak. Normalized intensity profiles were averaged over the entire circumferential arc to obtain representative transmural distributions, $I(x)$ where x is the distance from the extracted lumen and fit to the bell-shaped pattern predicted by a binding-diffusion model (Supplemental methods, Fig 2B)

$$I(x, t) = \exp\left(- \frac{x^2}{4D_{eff}t}\right) . \quad (3)$$

The derivation and numerical validation of Eq. 3 is provided in the Supplemental methods. For an inhomogeneous tissue, supplemental numerical simulations predict an exponential-like distribution that when fit to Eq. 3 provides an estimate of the spatially averaged effective diffusion coefficient (Fig S4F, Supplemental methods).

Histopathology and morphometry

Tubular segments (1-3 cm long) of untreated or OAS-treated arteries adjacent to ^{14}C-paclitaxel infused segments were formalin-fixed, resin embedded, step-sectioned at 5 μm, and stained with hematoxylin and eosin (H&E), and Movat pentachrome (MP). Qualitative parameters were assessed circumferentially in 30° arc increments as follows: *Predominate neointimal morphology* - (1) smooth muscle cells, (2) ground substance/mucinous elements, (3) fibrous tissue, (4) calcified, or (5) mixed morphology; *Mural* (i.e., neointima and tunica media combined) *and Tunica Media Calcification* - (1) < 25% wall thickness, (2) 25-50% wall thickness, (3) 50-75% wall thickness, (4) 100% wall thickness. Based on the incidence of neointimal calcification scores (i.e., a Score 4 as above), the circumferential extent of calcification was graded as (0) absence, (1) 0-25% of circumference, (2) 25-50%, (3) 50-75%, (4) 75-100%. Post-fluorescent analysis, frozen arterial sections were formalin-fixed and stained with H&E and/or MP. Using the approximate luminal centroid quantitative measurements of neointima and tunica media thickness were obtained circumferentially in 10° increments.

SEM

Arterial samples (3-5 cm long) explanted from transition regions that included both untreated and treated segments (Fig 1) were fixed in 2.5% glutaraldehyde and bisected longitudinally. Hemisections were rinsed with 0.1M sodium cacodylate buffer, post-fixed in 1% osmium tetroxide in 0.1M sodium cacodylate buffer, rinsed with 0.1M sodium cacodylate buffer and DI water, dehydrated in a graded series of alcohol solutions, dried using a critical point dryer, mounted onto metallic mounts, metal ion sputter coated, then examined and imaged at a range of magnifications with SEM (Hitachi, S3400-NII).

Statistics and data analysis

All data are presented as the mean ± standard error. Data fits to Eqs. 1 and 3 were performed using Matlab (MathWorks, Natick, MA, USA). Data were pooled either per segment, section or sector when considered appropriate. For all statistical tests, datasets were first assessed for normality using a Shapiro-Wilk test. For pairwise comparisons of continuous data, if normality was met, a t test was conducted; otherwise, a Mann-Whitney rank sum test was performed. Ordinal data (calcification scores) was compared using Mann-Whitney Rank Sums test. All statistical analyses were performed using Sigmaplot for Windows (Systat Software, San Jose, CA, USA) and the null hypothesis of no difference was only rejected if the value of the calculated statistic was ($p < 0.05$).

Results

Complimentary drug infusion experiments assessed OAS treatment effects on drug delivery. Infusion of ^{14}C-paclitaxel solutions enabled quantification of bulk drug absorption and its dependence on quadrant calcification scores (in 10 untreated and 9 OAS-treated segments). By contrast, infusion of fluorescently labeled drug solution enabled the quantification of distribution profiles and penetration depth relative to tissue ultrastructure markers (in untreated and 5 OAS-treated segments). Analysis of 3-D images and angiography revealed that femoropopliteal arterial segments assigned for radiolabeled drug infusion appeared less calcified than those assigned for fluorescent drug infusion (1.9±0.3 quadrants [absorption] vs 3.4±0.3 quadrants [distribution], p=0.006). Hence, though results from uptake and distribution studies are qualitatively similar and complimentary, the two data sets cannot be directly combined.

The effect of OAS treatment on arterial morphology and bulk drug absorption

The histopathologic appearance of untreated control femoropopliteal (n=5) and control tibial (n=2) segments was consistent with the morphology of atherosclerotic disease as typified by variable disruption of normal arterial architecture, frequent effacement/loss of the tunica media, and plaque formation (Fig 3A-C). Neointimal morphology was predominately collagenous/fibrous with varying lesser amounts of smooth muscle infiltration, extracellular matrix (i.e., proteoglycans), lipid, and/or calcification with highly variable thickness which was, on average, greatest in the popliteal segment. Plaque calcification in the popliteal segment was 2.7- and 4.6-fold greater relative to the SFA (p<0.001) and tibial (p<0.001) arteries, respectively. Medial calcification was observed in two tibial segments (6.4-fold relative to femoropopliteal segments, p<0.001). Regardless of artery, enface SEM of the luminal surface of untreated segments revealed variable endothelial coverage (Fig 3Ai-Ci). Plaque modifications related to OAS-treatment were evident by light microscopy of stained cross sections and enface SEM and characterized by variable denudation of endothelium and focally extensive disruption of subendothelial calcified plaque (Fig 3D-F). Relative to untreated controls, OAS-treated femoropopliteal segments exhibited decreases in plaque thickness (569.1±17.7μm [control] vs. 386.3±12.9μm [OAS], p<0.001) and calcified circumferential arc (19.0±4.9% [control] vs 10.5±2.8% [OAS], p=0.163).

Bulk absorption of ^{14}C paclitaxel in untreated segments was highly variable, ranging from 0.07-2.16 ng/mg (0.92±0.22 ng/mg, n=10). In OAS-treated segments, bulk paclitaxel absorption ranged from 0.52-2.49 ng/mg and trended 50% higher relative to untreated segments (1.38±0.20 ng/mg, n=9, p=0.147). Model based interpretation of tissue uptake normalized to perfusate dose (via Eq. 1) provided insights into the dependence of the bulk absorption rate-constant of ^{14}C paclitaxel (Eq. 2) on calcification scores and treatment. In untreated femoropopliteal segments the bulk absorption rate-constant decreased exponentially (5.5-fold per calcified quadrant) with increased calcium scores (p=0.05, n=7) (Fig 4). Moreover, paclitaxel absorption rates-constants were 461±451 fold higher in segments of the same artery when treated with OAS vs untreated Thus, the degree of circumferential calcification predicts arterial drug uptake and explains the large variability in this experimental cohorts.

Untreated arterial morphology and drug distribution profiles

Histologic assessment was performed on frozen sections to allow for co-registration of fluorescent drug distribution in the same tissue section. Untreated tissue segments used for fluorescent infusion studies revealed similarly developed atherosclerotic plaque morphologies (Fig 5A-C). In femoropopliteal and tibial segments, fluorescent intensity peaked at the luminal interface and exhibited large circumferential gradients that appeared to track with tissue morphology (Fig 5 Ai-Bi). Transmural fluorescent intensities declined to 10% of peak intensity within the plaque, 85.1 ± 2.1 μm from the luminal interface for SFA (415 sectors), 67.6 ± 2.3 μm for popliteal (381 sectors) and 48.0 ± 1.7 μm for tibial segments (203 sectors). Distribution curves appeared more exponential than bell-shaped (Fig 5Aii-Cii) consistent with a linearly increasing effective diffusion coefficient (Supplemental Methods, Fig S4), with spatial averages of $1.99\pm0.27\times10^{-9}$ cm^2/sec in the SFA (48 quadrants), $1.29\pm0.21\times10^{-9}$ cm^2/sec in popliteal (44 quadrants) and $0.59\pm0.07\times10^{-9}$ cm^2/sec in tibial segments (24 quadrants).

The effect of OAS treatment on drug distribution profiles

Qualitatively similar fluorescent distribution patterns were observed in OAS-treated arteries (Fig 6), with deepest penetration in the SFA (102.4 ± 2.1 μm, 895 sectors), 20% less in popliteal (81.7 ± 2.8 μm, 317 sectors, p<0.001) and 50% less in tibial segments (50.2 ± 1.7 μm, 306 sectors, p<0.001). Transmural distribution curves appeared more exponential than bell-shaped (Fig 6Aii-Bii), consistent with a linearly increasing effective diffusion coefficient (Supplemental Methods, Fig S4). OAS treated femoropopliteal segments exhibited 26% deeper paclitaxel penetration (p<0.001) and a 70% larger effective diffusion coefficient compared to untreated segments ($2.85\pm0.25\times10^{-9}$ cm^2/sec [treated] vs $1.66\pm0.18\times10^{-9}$ cm^2/sec [untreated], p<0.001). In tibial segments, the estimated effective diffusion coefficient was unchanged by OAS treatment ($0.64\pm0.06\times10^{-9}$cm^2/sec [treated] vs $0.59\pm0.07\times10^{-9}$ cm^2/sec [untreated], p=0.6).

Discussion

Arterial calcification has long been associated with poorer outcomes for endovascular drug delivery yet it remains unclear whether this is due to stent malapposition or hindrance of drug penetration and distribution after local release. *Ex-vivo* drug infusions of calcified arteries as in the current study provide a controlled model by which to directly study lesion barrier effects on drug distribution with and without lesion modification. Treated segments exhibited a trend for 50% greater ^{14}C-paclitaxel uptake of relative to control segments (1.38 ± 0.20 vs 0.92 ± 0.22 ng/mg, p=0.147). Treatment of femoropopliteal segments was associated with a ~180 μm reduction in plaque thickness (p<0.001) and a 45% reduction in circumferential intimal calcification (from 19.0 to 10.5%, p=0.163). These findings are well aligned with echogenicity analysis of IVUS estimated that OAS decreased the calcified area in the coronary artery of an arteriosclerosis obliterans patient by 58%[16] (from 11.0 to 4.6%). In concordance with these findings, fluorescent paclitaxel penetrated 26% deeper in OAS treated femorpopliteal segments compared to controls (p<0.001).

Mechanistic interpretation of experiments

A deeper understanding of the relationship between the two *ex-vivo* data sets and their significance to therapeutic scenarios was afforded via the development of a predictive model of arterial drug distribution based on the mechanism of diffusion and binding. The focus on these two processes was motivated by published *ex-vivo* and computational studies that illustrated their dominance in determining paclitaxel distribution and retention in healthy animal arteries[17–21]. The distribution patterns of fluorescent paclitaxel in human femoropopliteal segments were well explained by these processes when accounting for spatial variability in tissue composition, with a spatially averaged effective diffusion coefficient of, $1.7 \pm 0.2 \times 10^{-9}$ cm^2/sec at baseline and 70% higher in OAS-treated arteries (p<0.001). Notably, the published effective diffusion coefficient of paclitaxel in native porcine iliofemoral arteries[19] ($5.4 \pm 3.4 \times 10^{-7}$ cm^2/sec) is ~300-fold the estimate obtained in the current study, suggesting that mineralized plaque poses a more resistive barrier to paclitaxel distribution than healthy arterial tissue. Furthermore, the absorption rate-constant of ^{14}C-paclitaxel in untreated femorpopliteal segments exhibited log-linear decline with increasing calcium scores (Fig 4), decreasing 5.5-fold per calcified quadrant. As intimal calcification is predominately present in femoropopliteal arteries, these findings suggest that OAS enhancement of paclitaxel distribution in current experiments was mediated by a reduction in the degree of circumferential intimal mineralization which was less present in tibial arteries.

Implications for in vivo drug delivery

In vivo arterial wall distribution and retention are determined by a competition between binding and diffusion with luminal delivery and washout. For drug-eluting stents, drug release is typically sustained and rate limiting and washout is determined by stent geometry and degree of strut apposition and embedding[22, 23]. Inadequate stent apposition due to calcification will increase drug washout and limit drug distribution, particularly for a slow diffusing drug. In contrast, drug coated balloons present a drug-laden coating to the mural interface. Blood flow can spread this loosely adherent coating layer along the luminal interface or siphon and clear drug from the treatment site, concomitant with transmural diffusion of the drug into the artery wall. Thus, increased resistance to paclitaxel diffusion within the intima will result in increased washout and a potential reduction in efficacy.

As the rate of diffusion scales as the square root of the effective diffusion coefficient, the study data imply that the rate of paclitaxel distribution in intimal plaque is ~20-fold slower relative to healthy tissue, which can dramatically increase the degree of washout. These estimates imply that plaque modification that increases tissue permeability to drug will promote tissue drug retention and distribution.

Study limitations

The use of *ex-vivo* luminal drug exposures is an analytical convenience that does not seek to mimic the spatiotemporal dynamics of *in vivo* stent and balloon based drug delivery and cannot directly account for the presence of luminal clearance. Diffusion and binding of paclitaxel in cadaveric arterial tissue may not be fully representative of its transport in live

tissue and the quantitative validity of the findings is further limited by the use of labeled drug analogs. Yet, previously the *in vivo* drug distribution and retention following stent based and balloon based drug delivery were modeled successfully using parameter estimates derived from *ex-vivo* studies with radiolabeled analogs[19, 24]. Similarly, though OAS treatment may differentially affect plaque in live arteries vs cadaveric arteries, the estimated reduction in calcification in cadaveric femoropopliteal arteries (45%) is similar to the reported effects in fibrocalcific human coronary arteries[16].

As the main focus was on evaluation of drug delivery in calcified femoropoliteal arteries, limited observations on tibial segments and the experimental design do not allow conclusions to be drawn as to the influence of OAS treatment on drug transport in this differently structured anatomical and pathological vascular area. Thus, a different set of experiments is required to assess whether OAS affects paclitaxel distribution to tibial arteries.

Conclusions

Both experimental and modeling data support the hypothesis that intravascular delivery of paclitaxel is limited by the presence of calcified intimal plaque and may be enhanced via stromal modification by OAS-treatment. Whereas clinical success of atherectomy is typically measured by the degree of debulking and luminal gain, this study demonstrates that even more benign modification of calcified atherosclerotic plaque by OAS-treatment enhances drug transfer by increasing diffusion coefficient, thereby significantly enhancing adjunctive paclitaxel delivery. These data may explain the lack of responsiveness to balloon based delivery of paclitaxel in highly calcified peripheral arteries and suggest that the efficacy of such treatments may be safely enhanced via OAS treatment.

Supplementary Material

Refer to Web version on PubMed Central for supplementary material.

Acknowledgments

Abbreviations

OAS   orbital atherectomy system

IVUS   intravascular ultrasound

PAD   peripheral artery disease

PCB   paclitaxel coated balloon

SEM   scanning electron microscopy

SFA superficial femoral artery

References

1. Rocha-Singh KJ, Zeller T, Jaff MR. Peripheral arterial calcification: prevalence, mechanism, detection, and clinical implications. Catheter Cardiovasc Interv. 2014; 83:E212–220. [PubMed: 24402839]

2. Kashyap VS, Pavkov ML, Bishop PD, Nassoiy SP, Eagleton MJ, Clair DG, Ouriel K. Angiography underestimates peripheral atherosclerosis: lumenography revisited. J Endovasc Ther. 2008; 15:117–125. [PubMed: 18254670]

3. Fitzgerald PJ, Ports TA, Yock PG. Contribution of localized calcium deposits to dissection after angioplasty. An observational study using intravascular ultrasound. Circulation. 1992; 86:64–70. [PubMed: 1617791]

4. Adlakha S, Sheikh M, Wu J, Burket MW, Pandya U, Colyer W, Eltahawy E, Cooper CJ. Stent fracture in the coronary and peripheral arteries. J Interv Cardiol. 2010; 23:411–419. [PubMed: 20806458]

5. Micari A, Cioppa A, Vadala G, Castriota F, Liso A, Marchese A, Grattoni C, Pantaleo P, Cremonesi A, Rubino P, Biamino G. Clinical evaluation of a paclitaxel-eluting balloon for treatment of femoropopliteal arterial disease: 12-month results from a multicenter Italian registry. JACC Cardiovasc Interv. 2012; 5:331–338. [PubMed: 22440500]

6. Zeller T, Baumgartner I, Scheinert D, Brodmann M, Bosiers M, Micari A, Peeters P, Vermassen F, Landini M, Snead DB, Kent KC, Rocha-Singh KJ. Drug-eluting balloon versus standard balloon angioplasty for infrapopliteal arterial revascularization in critical limb ischemia: 12-month results from the IN.PACT DEEP randomized trial. J Am Coll Cardiol. 2014; 64:1568–1576. [PubMed: 25301459]

7. Fanelli F, Cannavale A, Gazzetti M, Lucatelli P, Wlderk A, Cirelli C, d'Adamo A, Salvatori FM. Calcium burden assessment and impact on drug-eluting balloons in peripheral arterial disease. Cardiovasc Intervent Radiol. 2014; 37:898–907. [PubMed: 24806955]

8. Tepe G, Beschorner U, Ruether C, Fischer I, Pfaffinger P, Noory E, Zeller T. Drug-Eluting Balloon Therapy for Femoropopliteal Occlusive Disease: Predictors of Outcome With a Special Emphasis on Calcium. J Endovasc Ther. 2015; 22:727–733. [PubMed: 26250747]

9. Akkus NI, Abdulbaki A, Jimenez E, Tandon N. Atherectomy devices: technology update. Medical devices. 2015; 8:1–10. [PubMed: 25565904]

10. Cioppa A, Stabile E, Popusoi G, Salemme L, Cota L, Pucciarelli A, Ambrosini V, Sorropago G, Tesorio T, Agresta A, Biamino G, Rubino P. Combined treatment of heavy calcified femoro-popliteal lesions using directional atherectomy and a paclitaxel coated balloon: One-year single centre clinical results. Cardiovasc Revasc Med. 2012; 13:219–223. [PubMed: 22632996]

11. Abdel-Wahab M, Baev R, Dieker P, Kassner G, Khattab AA, Toelg R, Sulimov D, Geist V, Richardt G. Long-term clinical outcome of rotational atherectomy followed by drug-eluting stent implantation in complex calcified coronary lesions. Catheter Cardiovasc Interv. 2013; 81:285–291. [PubMed: 22431433]

12. Abdel-Wahab M, Richardt G, Joachim Buttner H, Toelg R, Geist V, Meinertz T, Schofer J, King L, Neumann FJ, Khattab AA. High-speed rotational atherectomy before paclitaxel-eluting stent implantation in complex calcified coronary lesions: the randomized ROTAXUS (Rotational Atherectomy Prior to Taxus Stent Treatment for Complex Native Coronary Artery Disease) trial. JACC Cardiovasc Interv. 2013; 6:10–19. [PubMed: 23266232]

13. de Waha S, Allali A, Buttner HJ, Toelg R, Geist V, Neumann FJ, Khattab AA, Richardt G, Abdel-Wahab M. Rotational atherectomy before paclitaxel-eluting stent implantation in complex calcified coronary lesions: Two-year clinical outcome of the randomized ROTAXUS trial. Catheter Cardiovasc Interv. 2016; 87:691–700. [PubMed: 26525804]

14. Naito R, Sakakura K, Wada H, Funayama H, Sugawara Y, Kubo N, Ako J, Momomura S. Comparison of long-term clinical outcomes between sirolimus-eluting stents and paclitaxel-eluting stents following rotational atherectomy. International heart journal. 2012; 53:149–153. [PubMed: 22790681]

15. Tellez A, Dattilo R, Mustapha JA, Gongora CA, Hyon CM, Palmieri T, Rousselle S, Kaluza GL, Granada JF. Biological effect of orbital atherectomy and adjunctive paclitaxel-coated balloon therapy on vascular healing and drug retention: early experimental insights into the familial hypercholesterolaemic swine model of femoral artery stenosis. EuroIntervention. 2014; 10:1002–1008. [PubMed: 25308298]

16. Sotomi Y, Shammas NW, Suwannasom P, Campos CM, Wykrzykowska JJ, de Winter RJ, Dijkstra J, Serruys PW, Onuma Y. Impact of the Orbital Atherectomy System on a Peripheral Calcified Lesion: Quantitative Analysis by Intravascular Echogenicity. JACC Cardiovasc Interv. 2015; 8:e205–206. [PubMed: 26386765]

17. Creel CJ, Lovich MA, Edelman ER. Arterial paclitaxel distribution and deposition. Circ Res. 2000; 86:879–884. [PubMed: 10785510]

18. Hwang CW, Wu D, Edelman ER. Physiological transport forces govern drug distribution for stent-based delivery. Circulation. 2001; 104:600–605. [PubMed: 11479260]

19. Kolachalama VB, Pacetti SD, Franses JW, Stankus JJ, Zhao HQ, Shazly T, Nikanorov A, Schwartz LB, Tzafriri AR, Edelman ER. Mechanisms of tissue uptake and retention in zotarolimus-coated balloon therapy. Circulation. 2013; 127:2047–2055. [PubMed: 23584359]

20. Lovich MA, Creel C, Hong K, Hwang CW, Edelman ER. Carrier proteins determine local pharmacokinetics and arterial distribution of paclitaxel. J Pharm Sci. 2001; 90:1324–1335. [PubMed: 11745785]

21. Tzafriri AR, Levin AD, Edelman ER. Diffusion-limited binding explains binary dose response for local arterial and tumour drug delivery. Cell Prolif. 2009; 42:348–363. [PubMed: 19438899]

22. Balakrishnan B, Dooley J, Kopia G, Edelman ER. Thrombus causes fluctuations in arterial drug delivery from intravascular stents. J Control Release. 2008; 131:173–180. [PubMed: 18713645]

23. Balakrishnan B, Dooley JF, Kopia G, Edelman ER. Intravascular drug release kinetics dictate arterial drug deposition, retention, and distribution. J Control Release. 2007; 123:100–108. [PubMed: 17868948]

24. Tzafriri AR, Groothuis A, Price GS, Edelman ER. Stent elution rate determines drug deposition and receptor-mediated effects. J Control Release. 2012; 161:918–926. [PubMed: 22642931]

Clinical perspectives

Drug-eluting stents and drug-coated balloons have shown efficacy in treating peripheral artery disease, but calcific atherosclerosis remains a major and unexplained challenge to endovascular drug delivery treatments. More detailed knowledge of the barriers to drug distribution in diseased peripheral arteries forces derived from cadaveric models might be useful in guiding local drug delivery interventions in patients with calcified plaque to yield more consistent antirestenotic effects.
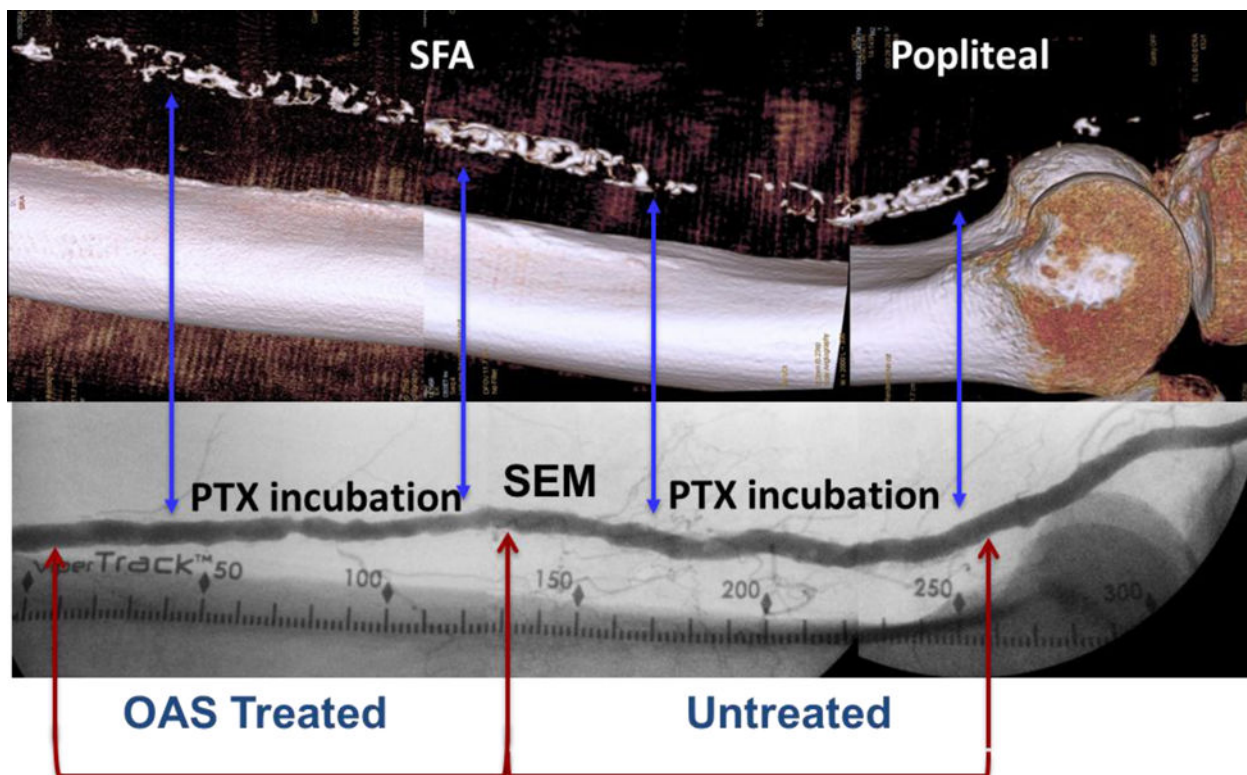
Figure 1. Experimental paradigm
Representative angiographic image (bottom) of the femoropopliteal artery illustrating treatment location and vessel segmentation. Segments assigned for fluorescent or radiolabeled drug infusion are demarcated by arrows (blue) and their corresponding calcium burden depicted in reconstructed 3-D images (top). Inserts depict cross section views along green demarcation arrows.
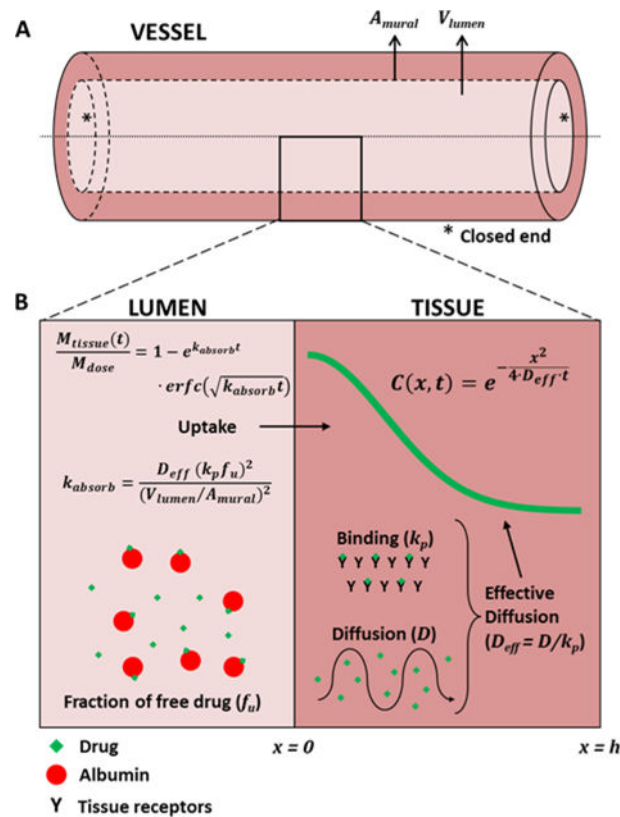
Figure 2. Schematic of diffusion-partitioning controlled arterial drug uptake and distribution
(A) Schematic of an excised arterial segment infused with drug solution and both ends were closed. V_{lumen} is the lumen volume and A_{mural} is the surface area of the infusate/tissue interface (B) High magnification cross sectional view of the lumen and arterial media, illustrating the key processes and equations governing drug distribution from a well-mixed infusate volume (V_{lumen}). In the lumen, a fraction f_u, if the drug is free and the remainder is bound to albumin). Only free drug is absorbed by the artery wall. Once in the tissue, free drug diffuses with diffusion coefficient D or binds nonspecifically to tissue proteins with partition coefficient k_p. Drug distribution is dominated by the effective diffusion coefficient D_{eff} (Eq. 3) whereas total drug uptake is also governed by the partition coefficient, lumen volume, mural area and the fraction of free drug (Eqs. 1–2).
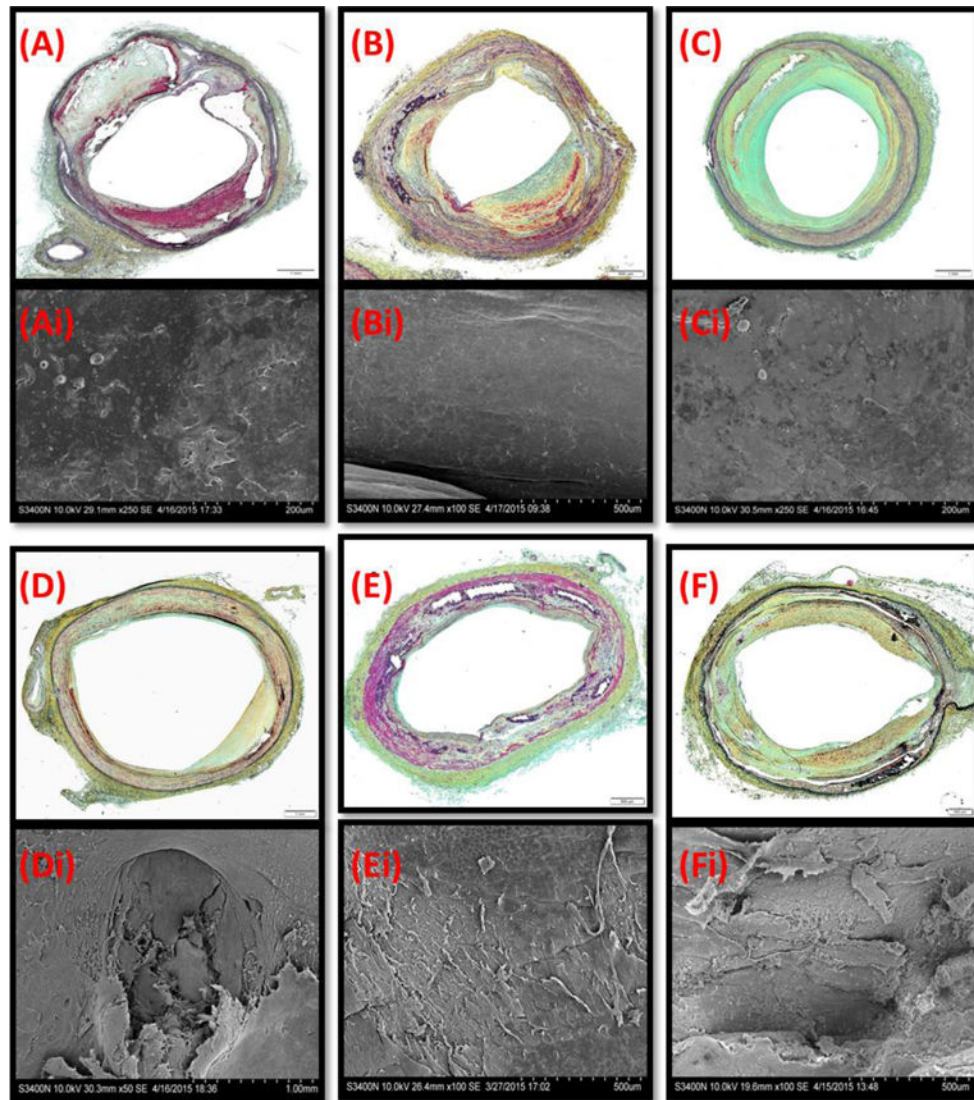
Figure 3. OAS treatment affects neointimal morphology
Representative MP stained cross sections (A-F) and matching enface SEM (Ai-Fi) of untreated (A-C) and OAS-treated (D-Fi) artery segments. (A,D) the SFA, (B,E) popliteal arteries, (C,F) tibial arteries.
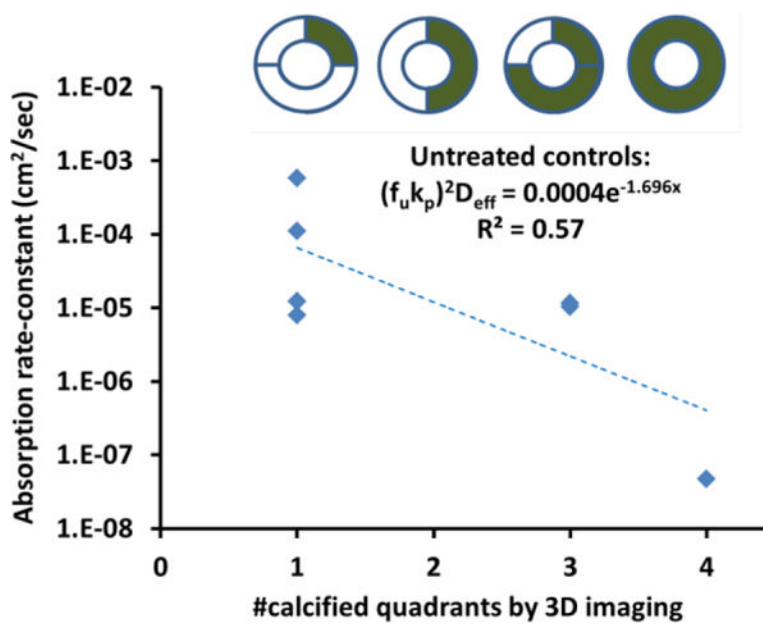
Figure 4. Paclitaxel absorption kinetics scale inversely with calcification scores
Bulk absorption rate-constants of paclitaxel (diamonds) decreased exponentially with increasing calcium scores in control femoropopliteal arteries.
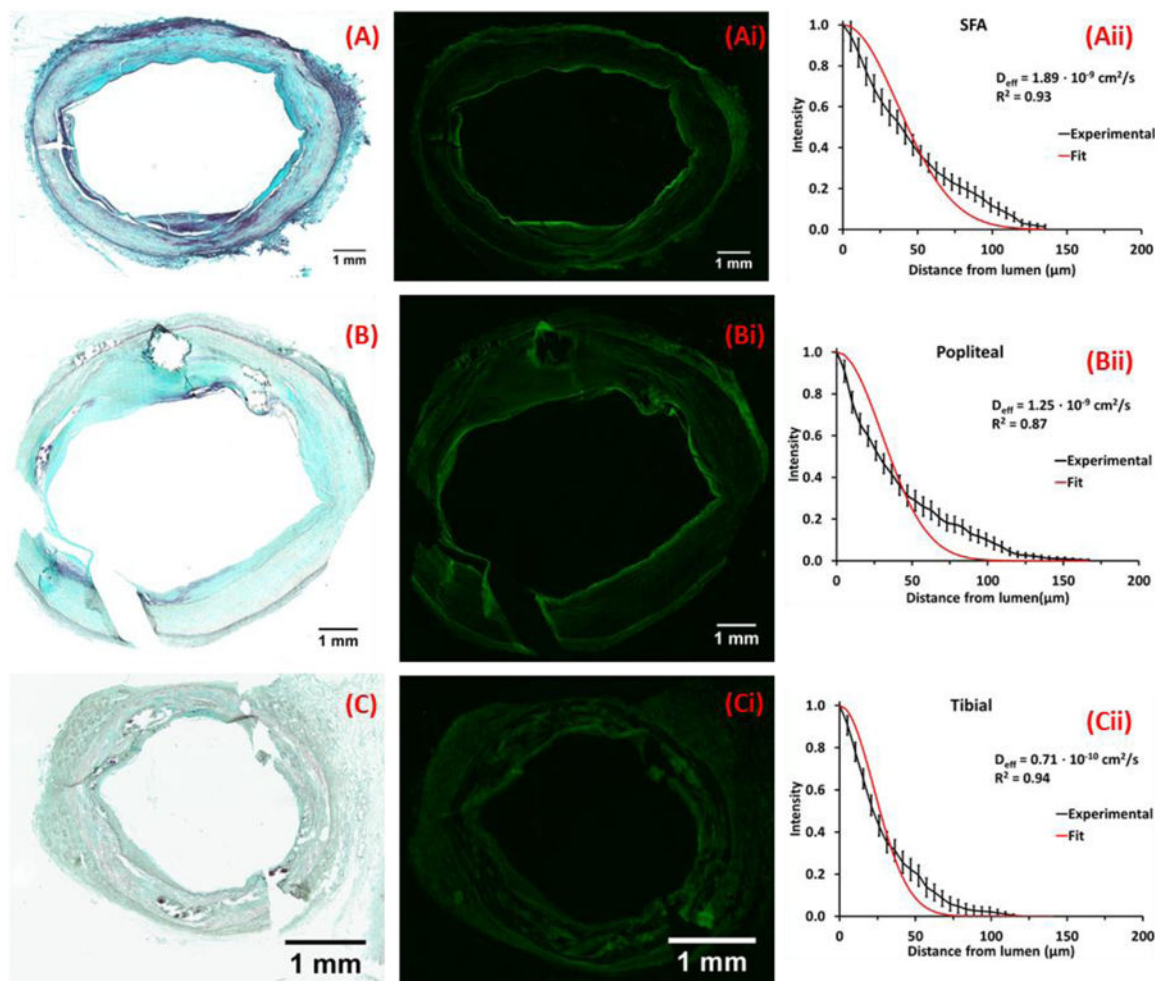
Figure 5. Morphology and drug distribution of representative untreated arterial segments
Representative MP stained frozen sections of the SFA (A) popliteal (B) and tibial (C)
arteries from a single leg; neointima thicknesses are respectively 372±166μm (A),
737±704μm (B) and 111±44μm (C). Corresponding fluorescent micrographs (Ai, Bi, Ci) and
normalized circumferentially averaged intensity plots (Aii, Bii, Cii) are depicted (black
lines) to the right of each micrograph along with best fit diffusion-binding predictions (red
line, Eq. 3). Best-fit effective diffusivities are respectively 1.90×10^{-9} cm^2/sec (A),
1.25×10^{-9} cm^2/sec (B) and 0.71×10^{-9} cm^2/sec (C).
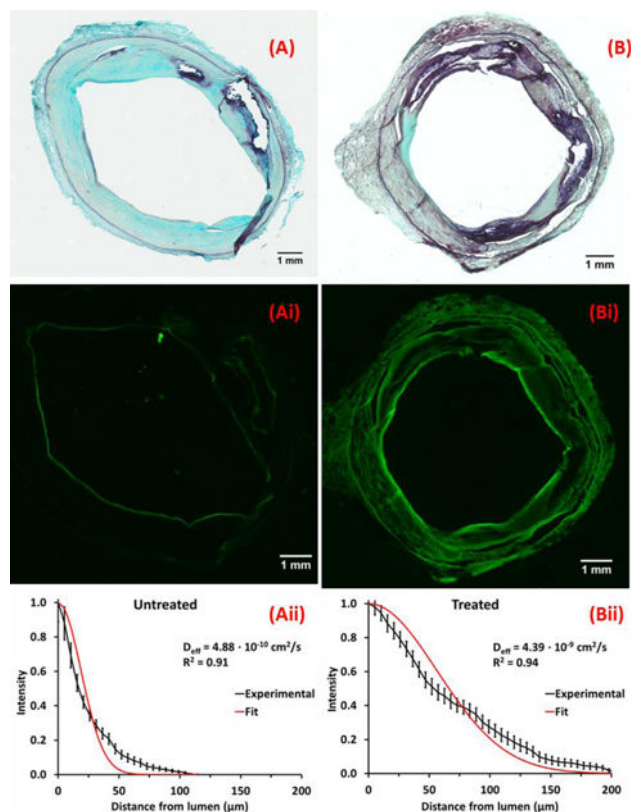
Figure 6. Morphology and drug distribution in control and OAS treated sections of a representative SFA

Representative MP stained frozen sections of untreated (A) and OAS-treated (B) SFA segments, and corresponding fluorescent micrographs (Ai, Bi) and normalized circumferentially averaged intensity plots (Aii, Bii, Cii) are depicted (black lines) to the right of each micrograph along with best fit diffusion-binding predictions (red line, Eq. 3). Intima thicknesses are 677±461μm (A) and 717±324μm (B). Best-fit effective diffusivities are 0.49×10^{-9} cm^2/sec (A), 4.39×10^{-9} cm^2/sec (B).